11-1-2023

Small molecule screen identifies pyrimethamine as an inhibitor of NRF2-driven esophageal hyperplasia

Brittany Bowman
Washington University School of Medicine in St. Louis
Julius Chembo
Washington University School of Medicine in St. Louis
M Ben Major
Washington University School of Medicine in St. Louis
et al.

Redox Biology 67 (2023) 102901

Contents lists available at ScienceDirect

Redox Biology

journal homepage: www.elsevier.com/locate/redox

Small molecule screen identifies pyrimethamine as an inhibitor of NRF2-driven esophageal hyperplasia

Chorlada Paiboonrungruang [a,b,1], Zhaohui Xiong [a,b,1], David Lamson [c], Yahui Li [a,b], Brittany Bowman [d], Julius Chembo [d], Caizhi Huang [b], Jianying Li [e], Eric W. Livingston [f], Jon E. Frank [f], Vivian Chen [b], Yong Li [g], Bernard Weissman [h], Hong Yuan [f,h,i], Kevin P. Williams [c,**], M. Ben Major [d,***], Xiaoxin Chen [a,b,j,k,l,*]

[a] Coriell Institute for Medical Research, Camden, NJ, 08103, USA
[b] Cancer Research Program, Julius L. Chambers Biomedical Biotechnology Research Institute, North Carolina Central University, Durham, NC, 27707, USA
[c] Department of Pharmaceutical Sciences, Biomanufacturing Research Institute and Technology Enterprise, North Carolina Central University, Durham, NC, 27707, USA
[d] Department of Cell Biology and Physiology, Department of Otolaryngology, Washington University in St. Louis, St. Louis, MO, 63110, USA
[e] Euclados Bioinformatics Solutions, Cary, NC, 27519, USA
[f] Biomedical Research Imaging Center, University of North Carolina, Chapel Hill, NC, 277599, USA
[g] Department of Thoracic Surgery, National Cancer Center, Cancer Hospital of Chinese Academy of Medical Sciences, Beijing, 100021, China
[h] Lineberger Comprehensive Cancer Center, University of North Carolina, Chapel Hill, NC, 277599, USA
[i] Department of Radiology, University of North Carolina, Chapel Hill, NC, 277599, USA
[j] Surgical Research Lab, Department of Surgery, Cooper University Health Care, Camden, NJ, 08103, USA
[k] MD Anderson Cancer Center at Cooper, Camden, NJ, 08103, USA
[l] Cooper Medical School of Rowan University, Camden, NJ, 08103, USA

ARTICLE INFO

Keywords:
Esophageal squamous cell carcinoma
NRF2
KEAP1
Pyrimethamine
Mitoxantrone

ABSTRACT

Objective: NRF2 is a master transcription factor that regulates the stress response. NRF2 is frequently mutated and activated in human esophageal squamous cell carcinoma (ESCC), which drives resistance to chemotherapy and radiation therapy. Therefore, a great need exists for NRF2 inhibitors for targeted therapy of NRF2^{high} ESCC.
Design: We performed high-throughput screening of two compound libraries from which hit compounds were further validated in human ESCC cells and a genetically modified mouse model. The mechanism of action of one compound was explored by biochemical assays.
Results: Using high-throughput screening of two small molecule compound libraries, we identified 11 hit compounds as potential NRF2 inhibitors with minimal cytotoxicity at specified concentrations. We then validated two of these compounds, pyrimethamine and mitoxantrone, by demonstrating their dose- and time-dependent inhibitory effects on the expression of NRF2 and its target genes in two *NRF2^{Mut}* human ESCC cells (KYSE70 and KYSE180). RNAseq and qPCR confirmed the suppression of global NRF2 signaling by these two compounds. Mechanistically, pyrimethamine reduced NRF2 half-life by promoting NRF2 ubiquitination and degradation in KYSE70 and KYSE180 cells. Expression of an *Nrf2^{E79Q}* allele in mouse esophageal epithelium (*Sox2CreER;LSL-Nrf2$^{E79Q/+}$*) resulted in an NRF2^{high} phenotype, which included squamous hyperplasia, hyperkeratinization, and hyperactive glycolysis. Treatment with pyrimethamine (30 mg/kg/day, *p.o.*) suppressed the NRF2^{high} esophageal phenotype with no observed toxicity.
Conclusion: We have identified and validated pyrimethamine as an NRF2 inhibitor that may be rapidly tested in the clinic for NRF2^{high} ESCC.

* Corresponding author. Coriell Institute for Medical Research, 403 Haddon Avenue, Camden, NJ, 08103, USA.
** Corresponding author. Department of Pharmaceutical Sciences and Biomanufacturing Research Institute and Technology Enterprise, North Carolina Central University, Durham, NC, 27707, USA.
*** Corresponding author. Department of Cell Biology and Physiology, Washington University in St. Louis, St. Louis, MO, 63110, USA.
E-mail addresses: kpwilliams@nccu.edu (K.P. Williams), bmajor@wustl.edu (M. Ben Major), lchen@coriell.org (X. Chen).
[1] Equal contribution to this research work.

https://doi.org/10.1016/j.redox.2023.102901
Received 27 July 2023; Received in revised form 19 September 2023; Accepted 21 September 2023
Available online 22 September 2023

1. Introduction

The development of human esophageal squamous cell carcinoma (ESCC) evolves through histological stages of hyperplasia, dysplasia, and carcinoma. The 5-year survival rate for ESCC is ~18%, a number that reflects late diagnosis, the aggressiveness of the disease, and a lack of effective treatment strategies [1,2]. Thus, there is a great need to further elucidate the molecular mechanisms driving the etiology of ESCC and develop more effective treatment strategies.

Nuclear factor (erythroid-derived 2)-like 2 (*NRF2* or *NFE2L2*) mutations are commonly seen in ESCC, with frequencies of 10–22% [3,4]. Mutations in other genes of the NRF2 signaling pathway, Kelch-like ECH-associated protein 1 (*KEAP1*) and Cullin 3 (*CUL3*), are present but less common than those in *NRF2*. *NRF2* mutations mainly occur in hotspots localized to the DLG and ETGE motifs, two domains required for NRF2 association with KEAP1, its primary inhibitor [5]. The NRF2 signaling pathway is recognized as a double-edged sword in the context of carcinogenesis [6,7]. On one hand, chemical or genetic activation of NRF2 induces cytoprotective enzymes conferring protection against chemical carcinogenesis in multiple models including esophageal cancer [8,9]. On the other hand, NRF2 activation mitigates stress associated with onco-metabolism, hypoxia, immune pressure, and aberrant proliferation. Indeed, NRF2 hyperactivation governs many of the cancer hallmarks, including cell proliferation, differentiation, immune infiltration, and cancer metabolism [10]. NRF2^{high} cancers of varied tissue origins demonstrate resistance to immune checkpoint inhibitors, chemotherapy, and radiation therapy [11,12]. In human ESCC, NRF2 overexpression significantly correlates with increased lymph node metastasis, postoperative recurrence, and decreased overall survival [13–16]. The NRF2 signaling pathway is regarded as a tractable molecular target for cancer therapy [17]. In mice, NRF2 hyperactivation in *Keap1*$^{-/-}$ mice results in esophageal hyperplasia and hyperkeratosis [18]. NRF2 is a critically important KEAP1 substrate as the esophageal phenotype of *Keap1*$^{-/-}$ mice is rescued in *Nrf2*$^{-/-}$*;Keap1*$^{-/-}$ and *K5Cre; Nrf2*$^{fl/fl}$*;Keap1*$^{-/-}$ mice [18,19].

Approximately 30 small-molecule NRF2 inhibitors have been reported [20,21]. While invaluable as tool compounds, these inhibitors have yet to be clinically proven. Continued and enhanced drug development efforts that identify potent, specific, and efficacious drugs for NRF2^{high} cancer are greatly needed. In this study, we used high-throughput small molecule screens to identify NRF2 inhibitors. We present data to validate two of these drugs, including mechanistic insights and *in vivo* efficacy in an NRF2^{high} genetically engineered mouse model (GEMM) of esophageal hyperplasia.

Abbreviations

CDDO	2-cyano-3,12-dioxo-oleana-1,9(11)-dien-28-oic acid
CHX	cycloheximide
CT	computed tomography
DEGs	differentially expressed genes
DHFR	dihydrofolate reductase
ESCC	esophageal squamous cell carcinoma
18F-FDG	18F-fluorodeoxyglucose
GFP	green fluorescent protein
GEMM	genetically engineered mouse model
IHC	immunohistochemical staining
IP	immunoprecipitation
KB	knowledge-based gene set
KEAP1	Kelch-like ECH-associated protein 1
MEEC	mouse esophageal epithelial cell
MIT	mitoxantrone
MTX	methotrexate
NRF2/NFE2L2	nuclear factor erythroid 2-related factor 2
PET	positron emission tomography
PYR	pyrimethamine
SUVmean	mean standardized uptake value
YFP	yellow fluorescent protein

2. Materials and methods

2.1. Cell culture and chemicals

NQO1-YFP H1299 cells (human lung adenocarcinoma), KYSE70 (*NRF2*^{W24C}), KYSE180 (*NRF2*^{D77V}) and KYSE450 (*NRF2*^{WT}) cells (human ESCC, DSMZ, Braunschweig, Germany) [20] were cultured in Gibco RPMI1640 GlutaMAX (ThermoFisher, Waltham, MA) supplemented with 10% FBS and 1% antibiotics (penicillin/streptomycin). *NQO1-YFP* H1299 cells contained a YFP fragment in *NQO1* intron 1 which responded to NRF2 activators [22]. Primary mouse esophageal epithelial cell (MEEC) was obtained from Dr. Scott Randel's lab (UNC-Chapel Hill). All cell lines were cultured in a humidified incubator at 37 °C with 5% CO_2.

The Prestwick library (1280 FDA-approved drugs) and Asinex library (34,560 compounds) were acquired from Prestwick Chemical (San Diego, CA) and Asinex (Winston-Salem, NC), respectively. Pyrimethamine (PYR), mitoxantrone dihydrochloride (MIT), brusatol, cycloheximide (CHX), methotrexate (MTX), and MG132 were purchased from Sigma-Aldrich (St. Louis, MO). All cell culture and biochemical assays were performed in duplicate or triplicate to ensure reproducibility.

2.2. High-throughput screening

NQO1-YFP H1299 cells were seeded at a density of 1000 cells/30 μl/well in 384-well plates using a Multidrop 384 (Thermo Fisher, Waltham, MA) bulk dispenser and cultured overnight. Individual compounds (1 μM in 0.1% DMSO) were added to wells using a Biomek NX workstation (Beckman-Coulter) (1 well per compound), with 0.1% DMSO as the positive control and an NRF2 activator (CDDO, 200 nM in 0.1% DMSO) as the negative control. All plates were monitored using the IncuCyte S3 (Essen BioScience, Ann Arbor, MI). Compounds that inhibited >50% of CDDO-activated signal (green GFP signal) and allowed >80% cell survival (red mCherry signal) were further examined in a dose-dependent experiment. Individual compounds were dispensed at 10-point serial dilutions starting from 10 μM in triplicate using an HP D300 Digital Dispenser (Hewlett-Packard, Palo Alto, CA). A known NRF2 inhibitor, brusatol, was used as a control. Plate image data was captured at 0, 24, 48, and 64 h and GraphPad Prism was used to analyze the dose-dependent screening data and calculate IC_{50}.

Cytotoxicity of 11 compounds (8 Prestwick compounds and 3 Asinex compounds) was tested in a dose-dependent screening assay. KYSE70 and KYSE180 cells were seeded at a density of 1200 cells/30 μl/well in 384-well plates and cultured overnight. Compounds were added to the plate at 2-point serial dilution in triplicate starting from 10 μM, with 0.1% DMSO as the negative control and 30 μM of benzethonium chloride as the positive control. After 3 days, another positive control was treated with 0.1% Triton X-100 right before staining. The viability of each well was assessed by double fluorescent staining with 0.5 μg/ml Hoechst and

100 nM YOYO1 (Invitrogen, Waltham, MA). Four images for each well were captured under 4× magnification using Thermo Scientific CellInsight NXT high-content screening platform. GraphPad Prism was applied to calculate both normalized total cell and dead cell percentages. IC_{50} values were calculated, and graphs generated for 11 compounds. PYR (an FDA-approved antimalarial and anti-toxoplasmosis drug targeting dihydrofolate reductase, DHFR) [23] and MIT (an FDA-approved chemotherapeutic drug) [24] were chosen for further validation because of their relatively potent NRF2-inhibitory activities and weak cytotoxic activities at the concentrations studied (Table 1).

2.3. Western blotting and immunoprecipitation (IP)

The nuclear and cytosolic extracts were prepared using a CelLytic NuCLEAR extraction kit (Sigma), and total protein (whole cell lysate) using RIPA buffer. Proteins were separated by SDS-PAGE and transferred to nitrocellulose membranes. Membranes were blocked and then incubated with a primary antibody overnight at 4 °C (Table S1). Chemiluminescence was detected using autoradiography film and followed by quantification using ImageJ.

To analyze NRF2 ubiquitination, cells were treated with a compound and then treated with or without MG132 (10 μM) before being harvested in RIPA buffer. The cell lysate was pre-cleaned with protein G agarose beads (Roche Diagnostic, Basel, Switzerland) for 1 h at 4 °C. Samples were incubated with 1 μg anti-NRF2 antibody overnight at 4 °C with rotation, and then 25 μl protein G agarose beads was added for 1.5 h at 4 °C. Immunoprecipitants were washed and boiled in 2X SDS loading buffer at 95 °C for 5 min, and analyzed by Western blotting with anti-ubiquitin.

2.3.1. Biochemical assays

A DHFR activity assay kit (Sigma) was used to analyze the enzymatic activity. The procedure was adjusted to a reaction volume of 200 μl. The reaction progress was followed by monitoring the decrease in A_{340nm} over time. MTX (1 μM) was used as a control DHFR inhibitor.

A protein synthesis assay kit (Cayman Chemicals, Ann Arbor, MI) was used to analyze global translation according to the manufacturer's instructions. KYSE70 cells were seeded at a density of 2000 cells/100 μl/well in a 96-well plate and treated with PYR, MIT, or CHX in triplicate (positive control). Cells were examined by ImageExpress Pico (Molecular Devices, San Jose, CA).

NRF2-ARE binding assays were performed with an ELISA-based TransAM NRF2 Assay Kit (Active Motif, Carlsbad, CA) according to the manufacturer's instructions. Briefly, nuclear extracts were prepared from untreated KYSE70 cells and added to the wells (20 μg/well) containing the ARE oligonucleotide. Then a competitor, a mutated competitor, PYR, or MIT was added to the wells. After incubation for 1 h with mild agitation and proper washing, anti-NRF2 antibody was added and incubated for 1 h. An HRP-conjugated secondary antibody and a substrate were added sequentially for measuring A_{450nm}.

NRF2 half-life was analyzed using CHX chase analysis. Cells were pre-incubated with PYR (10 μM), MIT (20 nM), or MTX (50 nM) for 4 h, followed by the addition of 200 μg/ml CHX to block protein synthesis. The cells were collected at the specified time points after CHX treatment. Total protein lysate was separated by SDS-PAGE and blotted with antibodies against NRF2 and GAPDH. Western blot images were quantified with ImageJ to calculate NRF2 half-life.

RNAseq was performed by Novogene (Durham, NC) and Admera Health (South Plainfield, NJ). Total RNA was used as input material for the RNA sample preparations. Sequencing libraries were generated using NEBNext Ultra TM RNA Library Prep Kit for Illumina (NEB, Ipswich, MA) following the manufacturer's recommendations and index codes were added to attribute sequences to each sample. After library preparation, the samples were sequenced (150 bp) according to manufacturer specifications. The quality-filtered reads were aligned with STAR (version 2.6.90c) to the human reference genome (hg38) with its respective RefSeq annotation, and the expression levels of genes were obtained with FeatureCounts (version 1.5.1). DESeq2 (version 1.34.1) was used to identify the differentially expressed genes (DEGs). Data matrices were normalized and the DEGs were reported according to the fold change cut-off and corrected modeling p-values. Gene set enrichment analysis was conducted to evaluate the differential enrichment of gene sets. Overall mRNA expression level of the NRF2 target genes was calculated using the RNAseq data at the natural log scale. The raw data has been submitted to the NCBI GEO database (GSE235584 and GSE235587). qPCR was performed to quantify the expression levels of genes of interest with relevant primers and TaqMan probes in a 96-well optical plate on an ABI 7900HT Fast Real-Time PCR system (Applied Biosystems).

2.4. Animal studies

All animal experiments were approved by the IACUC at North Carolina Central University (protocol number XC06142019). *Sox2CreER* mice and *LSL-Nrf2*$^{E79Q/+}$ mice [25] were crossed to express the *Nrf2*^{E79Q} mutant in the esophageal epithelium of adult *Sox2CreER;LSL-Nrf2*$^{E79Q/+}$ mice after tamoxifen induction (75 mg/kg/day, *i.p.*, 5 days). When the mice were sacrificed, BrdU (50 mg/kg, *i.p.*) was given 2 h before. A segment of the esophagus was harvested and fixed in formalin for histology, while esophageal epithelium and forestomach were stored in liquid nitrogen for molecular analyses.

Six mice were assessed by ^{18}F-FDG PET/CT at Week 0 (before tamoxifen induction) and Week 1 (after tamoxifen induction) following an established procedure [26]. In brief, each mouse was orally administered with a contrast agent (Iohexol, 150 mg/ml, 0.05 ml) under light anesthesia with isoflurane for visualization of the esophagus under

Table 1
Effects of 11 hit compounds on cell viability and NRF2 activity in H1299-YFP cells, and cell proliferation and cell death in *NRF2*^{Mut} ESCC cells (KYSE70 and KYSE180).

Compound	H1299-NQO1-YFP		KYSE70		KYSE180	
	Cell viability (IC_{50}, μM)	NRF2 inhibition (IC_{50}, μM)	Cell proliferation (IC_{50}, μM)	Cell death (IC_{50}, μM)	Cell proliferation (IC_{50}, μM)	Cell death (IC_{50}, μM)
Isoproterenol hydrochloride	>10	0.84	5.2	>10	>10	>10
Ethoxyquin	>10	0.29	>10	>10	>10	>10
Mitoxantrone dihydrochloride (MIT)	>10	0.035	0.00584	0.00324	0.00457	0.00522
Isoetharine mesylate	>10	0.49	>10	>10	>10	>10
Isoproterenol bitratrate	>10	0.43	4.9	>10	>10	>10
Pyrimethamine (PYR)	1.17	0.23	>10	14.6	13.7	>10
Triamterene	3.70	0.72	7.7	>10	>10	>10
Eseroline fumarate	>10	0.26	10	>10	>10	>10
Asinex 1	2.99	0.47	2.8	>10	3.2	>10
Asinex 2	4.87	0.04	6.3	>10	15.3	>10
Asinex 3	>10	1.21	5	>10	>10	>10

contrast-enhanced CT. About 350 μCi of ^{18}F-FDG was injected through a tail vein catheter. PET/CT imaging was conducted at 40 min post tracer injection under anesthesia. PET images were reconstructed using 3D-OSEM method with scatter, random, attenuation, and decay correction, and registered to the CT images of the same animal. The esophagus region was manually demarcated in CT images (highlighted by Iohexol) and superimposed on PET images. The mean standardized uptake value (SUV_{mean}) of ^{18}F-FDG was quantified in the esophagus of each mouse.

PYR was dissolved in N-methyl-2-pyrrolidone:PEG300 at the ratio of 1:9 for *in vivo* experiments. A dose-finding experiment was carried out in adult wild-type mice to determine the proper dose of PYR (15, 30, and 60 mg/kg, *p.o.,* 1/day for 4 weeks, n = 5 per group). Since myelosuppression is a common complication of PYR treatment in humans [27], we monitored general health (grooming, physical strength, and movement) and body weight during the treatment. Blood samples were collected for a complete blood count (IDEXX, Westbrook, ME).

Two experiments were performed to examine the therapeutic effect of PYR on the NRF2^{high} esophageal phenotype in the *Sox2CreER;LSL-Nrf2$^{E79Q/+}$* mice. In the first experiment, PYR was administered during tamoxifen induction (Fig. 5A). All tissue samples were collected at Week 5. In the second experiment, PYR was administered after tamoxifen induction (Fig. S6A). Part of the forestomach was harvested right after tamoxifen induction by surgical resection at Week 1, and the rest of the forestomach and esophageal epithelium were harvested when the mice were sacrificed at Week 3. Total protein was extracted from frozen tissues with a standard method for Western blotting. Total RNA was extracted from mouse esophageal epithelium for RNAseq. Paraffin sections were used for IHC of NRF2 and its target genes.

2.5. Histochemical and immunohistochemical staining (IHC)

Formalin-fixed tissues were processed, embedded in paraffin, and serially sectioned for staining. H&E staining was conducted using a routine protocol. For IHC, antigens were retrieved on the deparaffinized sections for detection with primary antibodies (Table S1) and further detected with a streptavidin-peroxidase reaction kit and DAB as a chromogen (ABC kit; Vector Labs, Burlingame, CA). To ensure the specificity of the primary antibody, control tissue sections were incubated in the absence of the primary antibody.

2.6. Statistical analysis

Z factor as a measure of screen assay quality was calculated according to an established method [28]. Data were presented as the mean ± SD after the quantitation of Western bands. GraphPad Prism 9 (GraphPad Software, La Jolla, CA) was used for Student's t-test. Complete blood counts were analyzed with an ANOVA test. Statistical significance was displayed as * $P < 0.05$, ** $P < 0.01$, and *** $P < 0.001$ unless indicated otherwise.

3. Results

3.1. High-throughput screening for NRF2 inhibitors

Using *NQO1*-YFP H1299 cells, we screened 35,840 chemical compounds at 1 μM (1280 from the Prestwick library and 34,560 from the Asinex library) with the YFP signal as an indicator of the NRF2 activity and the constitutively expressed mCherry red signal as an indicator of cell number and viability. The screen was performed at 64 h (Z' = 0.62). Eighteen compounds (1 μM) that inhibited >50% of the NRF2 activity and allowed at least 80% cell viability were selected for further analysis in a dose-response study using the same screening method. The list was narrowed down to 11 compounds that showed both potent NRF2-inhibitory activity and low toxicity on *NQO1*-YFP H1299 cells (Fig. 1 and Fig. S1).

We further analyzed their dose-dependent effects on the proliferation and cytotoxicity of KYSE70 and KYSE180 cells by high-content screening (Table 1, Fig. S2). Two compounds, PYR (IC_{50} = 0.23 μM) and MIT (IC_{50} = 0.035 μM), were chosen for further studies due to their potent NRF2-inhibitory effects and relatively low cytotoxicity. PYR is an FDA-approved anti-malarial and anti-toxoplasmosis drug targeting plasmodial DHFR at a concentration that is reported to be 1000 times less than that required to inhibit the mammalian enzyme [23]. MIT is approved by FDA for the treatment of numerous human cancers but not esophageal cancer [24].

3.2. PYR and MIT inhibited NRF2 expression in NRF2^{Mut} ESCC cells in vitro

NRF2^{Mut} ESCC cells (KYSE70 and KYSE180) were treated with PYR and MIT to validate their inhibitory effects on NRF2 expression. Both PYR and MIT inhibited the expression of nuclear NRF2 and cytoplasmic NQO1 in a dose- and time-dependent manner in KYSE70 cells (Fig. 2), as

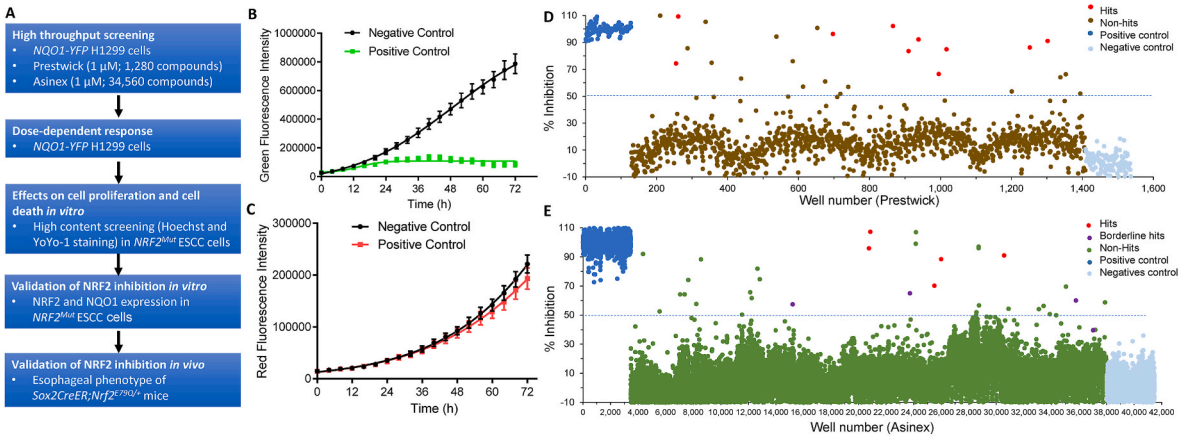

Fig. 1. High-throughput screening for NRF2 inhibitors from two compound libraries (1 μM) using *NQO1-YFP* H1299 cells. (A) Flow chart of the screening strategy; (B) Time-dependent changes of the YFP signal (NRF2 activity); (C) Time-dependent changes of the mCherry signal (cell viability); Negative control: exposure to a known NRF2 activator (CDDO, 200 nM); Positive control: exposure to the vehicle. (D) Prestwick library (1280 FDA-approved drug compounds); (E) Asinex library (34,560 compounds). Hit compounds were selected if the CDDO-induced NRF2 activity was inhibited by >50% and cell survival was >80%. Three compounds from the Asinex library were defined as borderline hits because their inhibition of NRF2 activity was >50%, yet their effects on cell survival were ~80%.

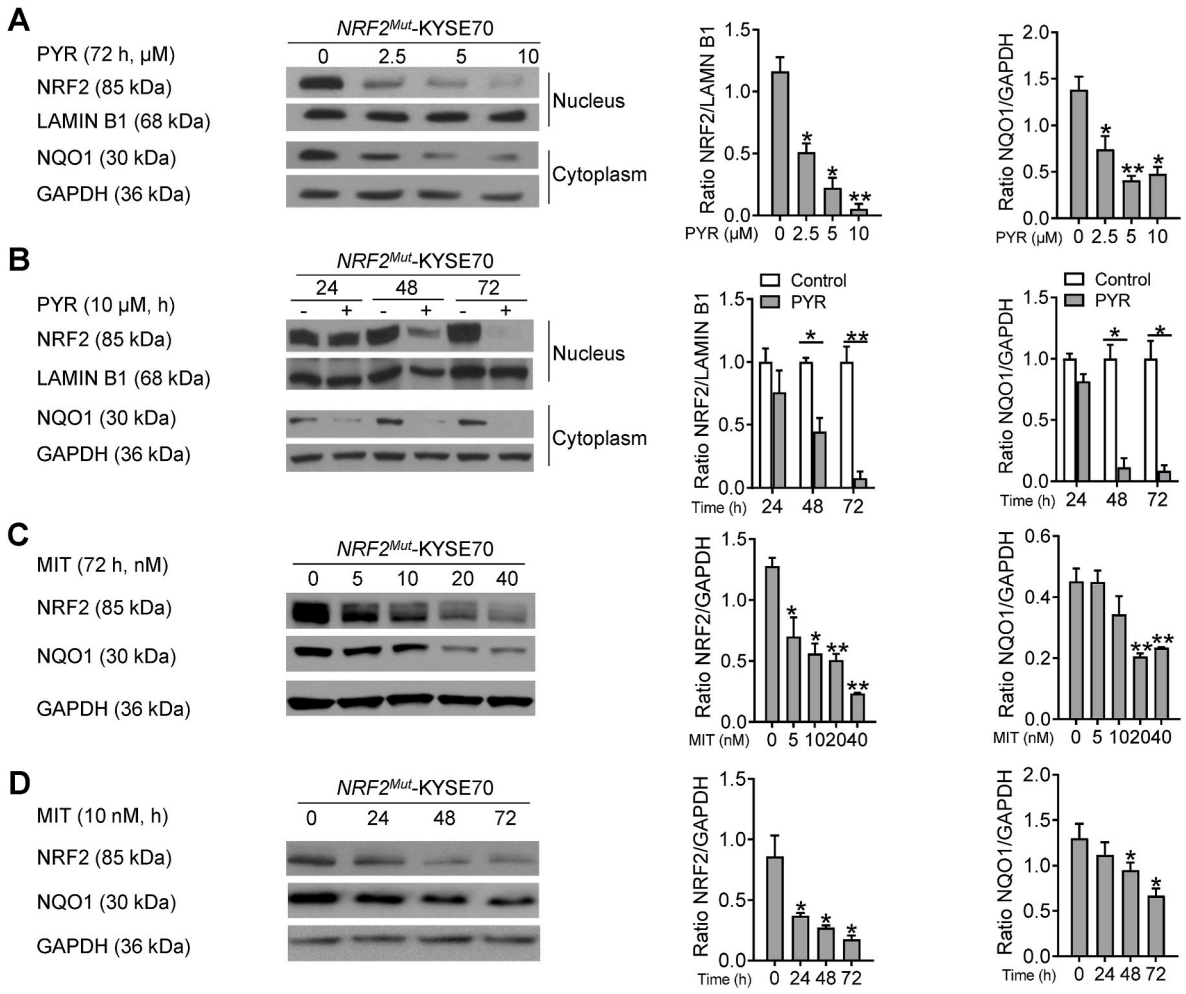

Fig. 2. PYR and MIT downregulated NRF2 and NQO1 expression in *NRF2*^{Mut}-KYSE70 cells in a dose- and time-dependent manner. (A) Dose-dependent downregulation of the expression of nuclear NRF2 and cytoplasmic NQO1 by PYR; (B) Time-dependent downregulation of the expression of nuclear NRF2 and cytoplasmic NQO1 by PYR (10 μM); (C) Dose-dependent downregulation of NRF2 and NQO1 expression by MIT; (D) Time-dependent downregulation of NFR2 and NQO1 expression by MIT (10 nM). *$P < 0.05$, **$P < 0.01$.

well as in KYSE180 cells (Fig. S3).

Principal component analysis of RNAseq data showed that PYR-treated samples, MIT-treated samples and control samples were clustered separately, suggesting distinct effects of PYR and MIT on the global mRNA expression pattern in KYSE70 cells (Fig. S4A). Human NRF2 target gene set was negatively enriched in PYR and MIT-treated cells (Fig. S4B). The overall mRNA expression level of human NRF2 target genes in KYSE70 cells was significantly reduced by PYR (10 μM for 72 h) and MIT (20 nM for 72 h) (Fig. S4C) (Excel S1). Furthermore, PYR had a negative impact on 54 canonical pathways, while MIT affected 65. Conversely, PYR positively influenced 79 canonical pathways, and MIT influenced 86 in a positive manner. Likewise, PYR negatively impacted 68 gene ontology pathways, while MIT affected 121 negatively. On the other hand, PYR positively influenced 143 gene ontology pathways, while MIT had a positive impact on 76. Notably, both PYR and MIT treatments exhibited significant modulation of numerous metabolism and cancer-associated pathways. Evidently, both PYR and MIT exert a wide range of effects on gene expression across multiple molecular pathways.

qPCR confirmed the downregulation of *NFE2L2* mRNA (Fig. S4D) and several NRF2 target genes (*AKR1B10, AKR1C2, AKR1C3, PGD, SLC7A11, TKT*) by PYR and MIT (Fig. S4E). Interestingly, PYR treatment upregulated NRF2 expression in both *Nrf2*^{WT} mouse esophageal epithelial cells (MEEC) and *NRF2*^{WT} ESCC cells (KYSE450) (Figs. S4F–G). These results demonstrated that PYR inhibited NRF2 expression and transcriptional activity in *NRF2*^{Mut} ESCC cells *in vitro* in a relatively specific manner.

3.3. Biochemical effects of PYR and MIT on human ESCC cells in vitro

Since PYR was recently reported to inhibit DHFR and STAT3 in human cancer cells [29,30], we evaluated whether PYR inhibited STAT3 and DHFR activity in human ESCC cells. In KYSE70 cells, PYR (up to 10 μM) did not significantly inhibit pSTAT3 and STAT3 expression (Fig. S5A), but did significantly inhibit DHFR activity starting at 5 μM (Fig. S5B). A known DHFR inhibitor (MTX) significantly inhibited NRF2 expression in both *NRF2*^{Mut}-KYSE70 and *NRF2*^{WT}-KYSE450 cells (Figs. S5C–D).

Although MIT was reported to inhibit topoisomerase II and the expression of ABCG2 [31], MIT increased ABCG2 and TOP2A expression in KYSE70 cells (Figs. S5E–F). Because some small molecule NRF2 inhibitors (e.g., brusatol and halofuginone) suppressed global translation [32,33], we next examined whether PYR and MIT inhibited global translation using a protein synthesis assay with CHX as a positive control. Neither PYR (10 μM) nor MIT (20 nM) inhibited global translation (Fig. S5G). We also examined the effects of PYR or MIT on NRF2-ARE binding activity in KYSE70 cells and did not observe any changes (Fig. S5H).

Since disruption of NRF2-KEAP1 interaction due to stress or gene mutations extends the half-life of the short-lived NRF2^{WT} (half-life =

~20min [34]), we examined the effects of PYR and MIT on NRF2 half-life. CHX chase experiments showed that PYR (10 μM) and MIT (20 nM), but not MTX (50 nM), significantly shortened NRF2 half-life in *NRF2*^{Mut}-KYSE70 from 66.7 min to 34.9 min and 42.7 min, respectively (Fig. 3A). Similarly, PYR (10 μM) and MIT (20 nM) shortened NRF2 half-life in *NRF2*^{Mut}-KYSE180 cells (Fig. 3B), but not in *NRF2*^{WT}-KYSE450 cells (Fig. 3C).

We next investigated the effects of PYR and MIT on NRF2 ubiquitination and degradation. Using NRF2-IP and ubiquitin western blotting, we found that PYR (10 μM), but not MIT (20 nM), promoted NRF2 ubiquitination in the presence of MG132 (a proteasome inhibitor) in KYSE70, KYSE180, and KYSE450 cells (Fig. 3D–F). Taken together, our data suggested that PYR may inhibit NRF2 expression in *NRF2*^{Mut} ESCC cells by promoting NRF2 ubiquitination and degradation, and thus reducing NRF2 half-life.

3.4. NRF2-inhibitory effects of PYR on the NRF2^{high} esophageal phenotype in vivo

We chose to test the *in vivo* efficacy of PYR instead of MIT because PYR has recently been tested in clinical trials on cancer. PYR has a better safety profile than MIT and cytotoxicity of MIT may complicate the analysis. A mouse model was first established by expressing a mutant allele in the mouse esophagus (*Sox2CreER;LSL-Nrf2*$^{E79Q/+}$) (Fig. 4A). Our previous experiment using the *K14Cre;LSL-Nrf2*$^{E79Q/+}$ mice has shown that expression of the mutant allele resulted in squamous epithelial hyperplasia in the tongue, esophagus, and forestomach [25]. Four weeks after tamoxifen induction, NRF2, NRF2 transcriptional targets (GCLC, GCLM) and a keratinization marker (Loricrin) were overexpressed in the mutant esophagus, as detected by Western blotting and IHC (Fig. 4B–C). An increased number of BrdU^{+} cells and increased thickness of the keratinized layer indicated hyperplasia and hyperkeratosis of the esophageal squamous epithelium. At Week 6, mild dysplasia developed (Fig. 4C). However, up to 20 weeks after tamoxifen induction, no tumors were found in the mouse esophagus (data not published), suggesting that NRF2 activation likely drives cancer progression but not cancer initiation. Using ^{18}F-FDG PET/CT, we further found that this mutant allele resulted in hyperactive glycolysis (increased ^{18}F-FDG uptake) after tamoxifen induction (Fig. 4D).

Using three doses of PYR (15, 30, and 60 mg/kg/day) in adult wild-type mice, we did not observe any negative impact on the body weight and general health of the mice. However, PYR at the dose of 60 mg/kg/day resulted in myelosuppression including leukopenia and lymphopenia (Table S2). Thus, we chose 30 mg/kg/day *p.o.* as the dose for subsequent experiments to investigate the NRF2-inhibitory effects of PYR on the NRF2^{high} esophageal phenotype in our mouse model.

In the first animal experiment, PYR was given together with tamoxifen (Fig. 5A). PYR (30 mg/kg/day, *p.o.*, for 5 weeks) reduced the expression of NRF2 and NRF2 target genes (GCLC, GCLM, PKM2) and a cell proliferation marker (BrdU incorporation) which was upregulated by the mutant allele, as detected by western blotting and IHC (Fig. 5B–C). In the second animal experiment, PYR was given after tamoxifen induction (Fig. S7A). RNAseq data showed that PYR significantly inhibited the overall mRNA expression level of mouse NRF2 target genes in the esophageal epithelium (Fig. S7B) (Excel S2). In the esophageal epithelium, PYR significantly inhibited the expression of NRF2 and its target genes (HMOX1 and AKR1C3). NQO1, GCLC and GCLM expression in the esophageal epithelium were inhibited, yet without statistical significance. However, it remains unclear why one mouse did not respond to PYR treatment. In the forestomach, NRF2 expression was significantly inhibited by PYR as well (Fig. S7C).

4. Discussion

We identified multiple potential NRF2 inhibitors using high-throughput screening of small molecule compound libraries. Because of its low toxicity in humans and the absence of studies testing efficacy in patients with cancer, we characterized the effects of PYR on NRF2 using ESCC cells and GEMM.

PYR inhibits plasmodial DHFR [23] and STAT3 in leukemia cells [29], down-regulates mutant Cu/Zn superoxide dismutase (an NRF2 transcriptional target) in the cerebrospinal fluid of amyotrophic lateral

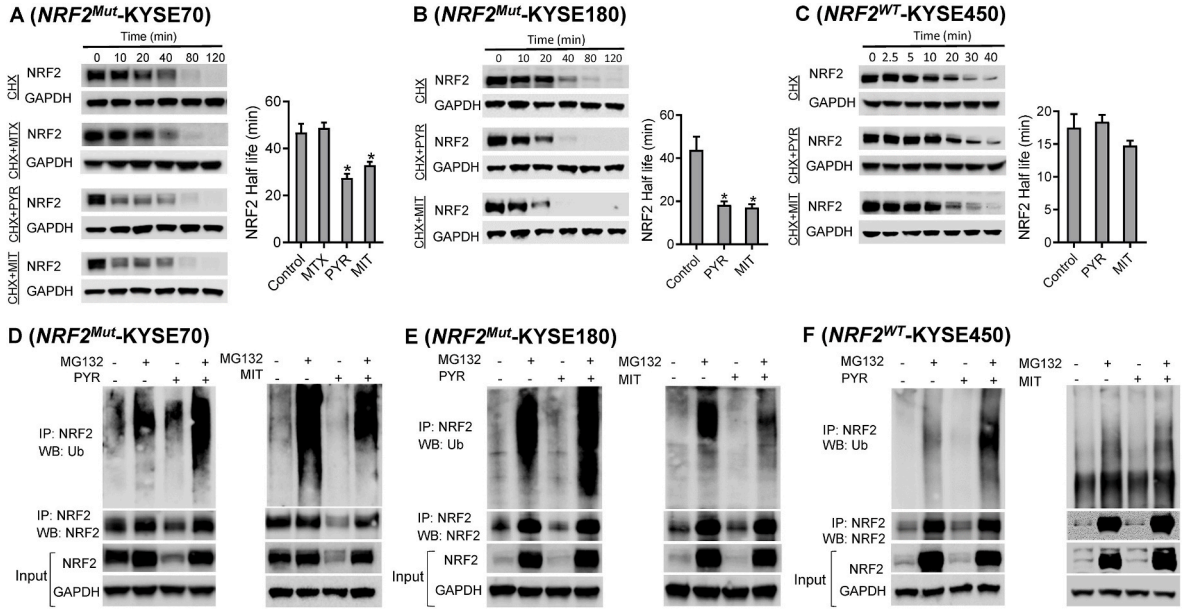

Fig. 3. PYR shortened NRF2 half-life and promoted NRF2 ubiquitination in *NRF2*^{Mut} ESCC cells. (A) NRF2 half-life was shortened by PYR (10 μM) and MIT (20 nM), but not by MTX (50 nM), in *NRF2*^{Mut}-KYSE70 cells. (B) NRF2 half-life was reduced by PYR (10 μM) and MIT (20 nM) in *NRF2*^{Mut}-KYSE180 cells. (C) NRF2 half-life was not changed by PYR (10 μM) and MIT (20 nM) in *NRF2*^{WT}-KYSE450 cells. (D) PYR (10 μM), but not MIT (20 nM), promoted NRF2 ubiquitination in *NRF2*^{Mut}-KYSE70 cells in the presence or absence of MG132 (a proteasomal inhibitor). (E) PYR (10 μM), but not MIT (20 nM), promoted NRF2 ubiquitination in *NRF2*^{Mut}-KYSE180 cells in the presence or absence of MG132. (F) PYR (10 μM), but not MIT (20 nM), slightly promoted NRF2 ubiquitination in *NRF2*^{WT}-KYSE450 cells only in the presence of MG132. *$P < 0.05$.

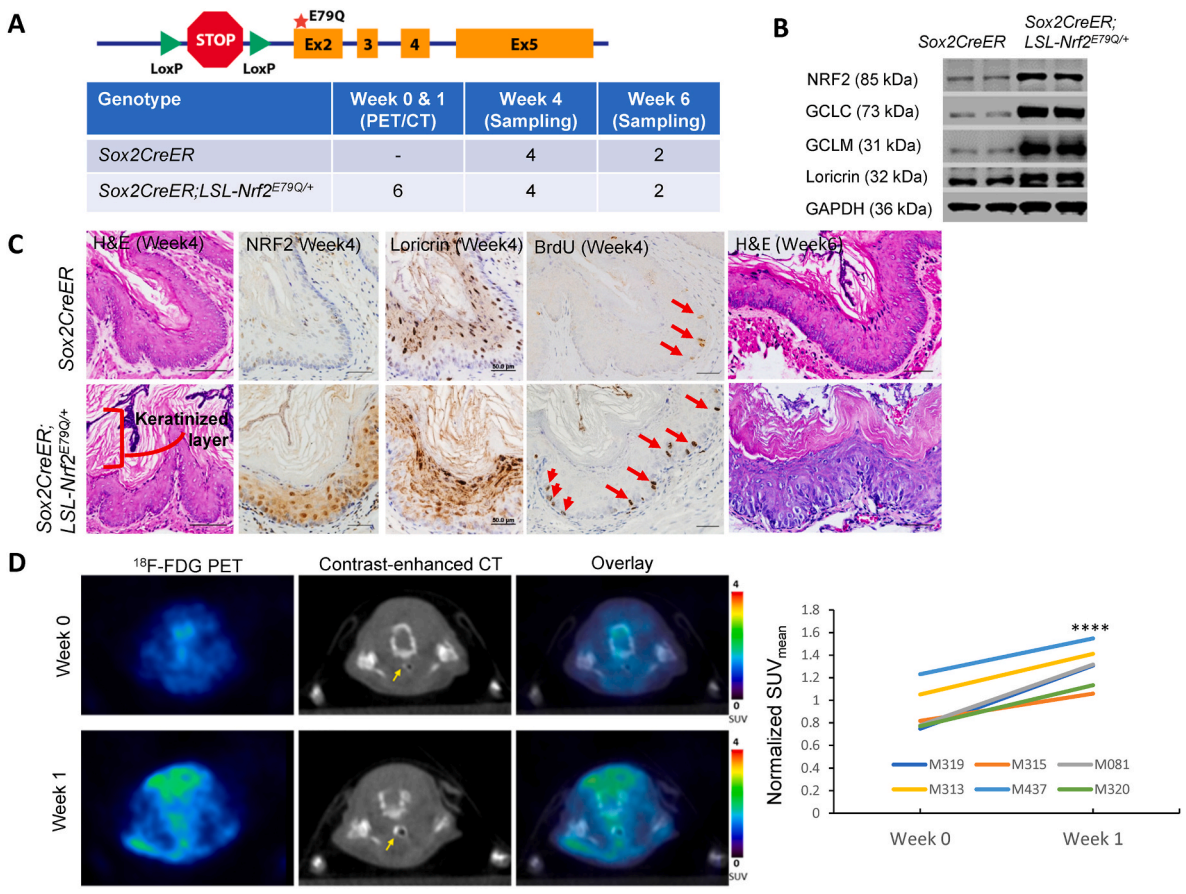

Fig. 4. NRF2^{high} esophageal phenotype in *Sox2CreER;LSL-Nrf2*$^{E79Q/+}$ mice. (A) Schematic figure of the *LSL-Nrf2*^{E79Q} allele and experimental design. (B) Expression of NRF2, NRF2 target genes (GCLC and GCLM), and a keratinization marker (loricrin) in the esophageal epithelium of *Sox2CreER;LSL-Nrf2*$^{E79Q/+}$ mice as detected with Western blotting; (C) Histology of the esophageal epithelium at 4 and 6 weeks after tamoxifen activation (H&E) and expression of NRF2, loricrin, and a proliferation marker (BrdU) in the mouse esophageal epithelium as detected with IHC. (D) ^{18}F-FDG PET/CT of mouse esophagus before tamoxifen induction (Week 0) and after tamoxifen induction (Week 1). Transverse views of the esophagus (arrow, highlighted by the contrast agent) of one mouse (M313) are shown. ****$P < 0.001$.

sclerosis patients [35], and suppresses the growth of various cancer cells [36–40]. In *NRF2*^{Mut} ESCC cells, PYR inhibited NRF2 expression in a dose- and time-dependent manner (Fig. 2, S3). RNAseq and qPCR data confirmed the downregulation of NRF2 signaling (Fig. S4). We excluded inhibition of STAT3, global translation, and NRF2-ARE binding, as possible mechanisms of action in our experimental system (Fig. S5). Instead, we found PYR promoted NRF2 ubiquitination and degradation, and thus shortened its half-life in *NRF2*^{Mut} ESCC cells (Fig. 3).

In agreement with a previous study [41], we also identified MIT as a candidate NRF2 inhibitor. Although it did not impact NRF2 ubiquitination, it did shorten NRF2 half-life (Fig. 3). MIT is FDA-approved for the treatment of numerous human cancers, but not yet for esophageal cancer [24]. It has been reported to induce transitory subjective and objective response without significant local or systemic side effects in five patients with inoperable, recurrent esophageal cancer after local administration [42]. Mechanistically, MIT mainly acts through intercalation with the DNA molecule, which in turn causes single- and double-stranded disruptions and suppresses DNA repair via inhibition of topoisomerase II. It can also intercalate with GC-rich mRNAs (e.g., *HIF1α, tau* pre-mRNA) [43,44] and interact with proteins (e.g., PIM1 kinase) and lipids non-covalently [24]. Since the promoter of *NFE2L2* mRNA is very GC-rich [45], interference with *NFE2L2* mRNA translation may be a mechanism of action. C_{max} of MIT in the plasma reached as high as 6.43 ± 2.43 mg/L (12.43 ± 4.70 μM) at the dose of 90 mg/m^2 after intravenous injection. Plasma concentration of MIT remained as high as 4.65 ± 2.35 μg/L (8.99 ± 4.54 nM) at 96 h after injection [46]. Therefore, the concentrations used in this study are clinically achievable. Further studies are warranted to elucidate MIT's mechanisms of action and its NRF2-inhibitory effect *in vivo*.

Five strategies have been proposed to target the NRF2 signaling pathway for cancer therapy: (1) transcriptional downregulation of *NRF2*; (2) increased degradation of *NRF2* mRNA or decreased translation; (3) enhancement of NRF2 degradation through up-regulation/activation of KEAP1-CUL3, β-TrCP-SCF or HRD1; (4) blocking the dimerization of NRF2 with small MAF proteins; and (5) blocking the NRF2-sMAF DNA-binding domain [47]. Our data suggest that small molecules (e.g., PYR) may inhibit NRF2 by promoting its ubiquitination and degradation. Consistent with our data, PYR has been reported to promote ubiquitination and degradation of AIMP2-DX2 in lung cancer cells [48]. These data suggest that studies on the NRF2 protein degradation mechanism of PYR may further elucidate its mechanism of action. On the other hand, antimetabolites (e.g., MTX) have been reported to inhibit NRF2 [49]. DHFR inhibition was reported as a mechanism of action of PYR on lung cancer cell proliferation [30]. In this study, both DHFR inhibitors (PYR and MTX) inhibited NRF2 expression in *NRF2*^{Mut} cells. However, PYR upregulated NRF2 expression (Figs. S4F–G), whereas MTX downregulated its expression, in *Nrf2*^{WT} cells, suggesting that PYR is relatively specific for mutant NRF2, and has a DHFR-independent effect.

The most exciting observation is that PYR effectively inhibited the NRF2high esophageal phenotype in mice. Upon tamoxifen induction, *Sox2CreER;LSL-Nrf2*$^{E79Q/+}$ mice developed typical NRF2high

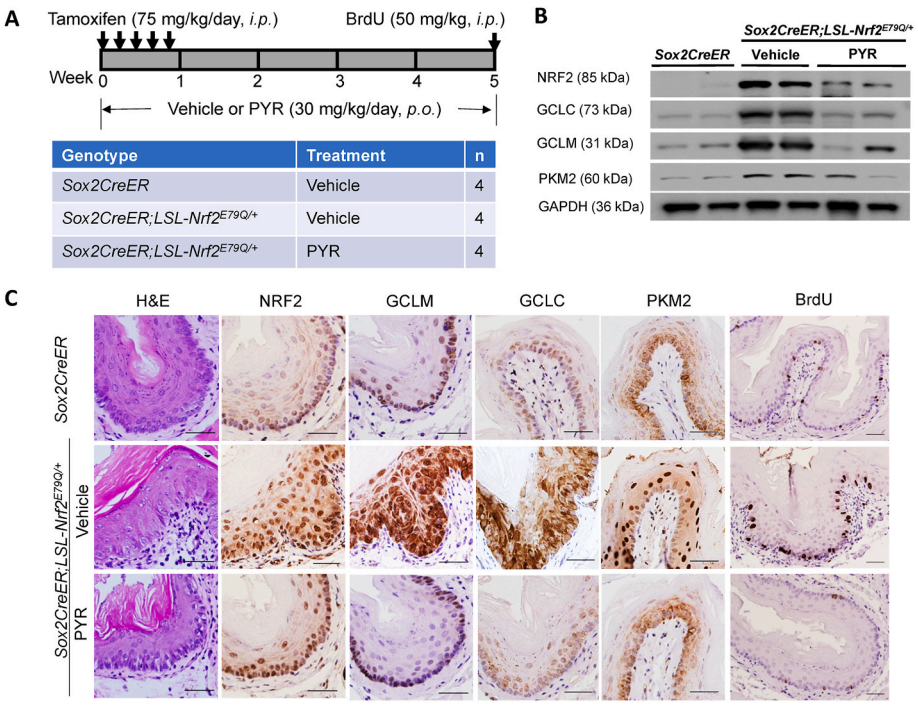

Genotype	Treatment	n
Sox2CreER	Vehicle	4
Sox2CreER;LSL-Nrf2$^{E79Q/+}$	Vehicle	4
Sox2CreER;LSL-Nrf2$^{E79Q/+}$	PYR	4

Fig. 5. PYR inhibited NRF2 expression in the esophageal epithelium of *Sox2CreER;LSL-Nrf2*$^{E79Q/+}$ mice. (A) Experimental design to test the effect of PYR (30 mg/kg/day, *p.o.*) on the NRF2^{high} phenotype in the mouse esophagus; (B) Expression of NRF2 and its target genes (GCLC, GCLM, PKM2) in the esophageal epithelium of *Sox2CreER;LSL-Nrf2*$^{E79Q/+}$ mice as detected with Western blotting; (C) Histology and expression of NRF2, NRF2 target genes, and BrdU in the esophageal epithelium of *Sox2CreER;LSL-Nrf2*$^{E79Q/+}$ mice as detected with IHC. Scale bar = 50 μm.

esophageal phenotype (hyperplasia, hyperkeratosis, and overexpression of NRF2 and its target genes) as reported in *Keap1*−/− mice [18] (Figs. 4 and 5). Consistent with the phenotype of hyperactive glycolysis in *Keap1*−/− esophagus [50], expression of the *Nrf2*^{E79Q} mutant significantly increased 18F-FDG uptake in the mouse esophagus (Fig. 4D). Cmax of PYR was reported as high as 8.04, 18.5, 35.78, and 28.15 μM when given to mice at the dose of 12.5, 25, 50, and 75 mg/kg, *i.p.* [51]. Thus, 30 mg/kg/day is expected to achieve a concentration of ~10 μM in mouse tissues. At this dose, PYR was not myelosuppressive (Table S2), yet significantly inhibited the expression of NRF2 and its target genes in the esophageal epithelium and forestomach (Fig. 5B, C, S7B, S7C). In humans, the Cmax of PYR reached 8.28 μM after 50 mg/day, *p.o.*, for 3 weeks [38]. These data suggest that PYR can be an NRF2 inhibitor with a good safety profile for humans.

In summary, using a small molecule screen we have identified PYR as an NRF2 inhibitor, and further validated it as an inhibitor of NRF2 expression *in vitro* and *Nrf2*^{Mut}-driven esophageal hyperplasia *in vivo*. The NRF2-inhibitory effect of PYR at a clinically achievable and safe dose suggests that PYR is a promising NRF2 inhibitor that may be rapidly tested in the clinic for human *NRF2*^{Mut} ESCC. Further exploration of its mechanisms of action may lead to more potent NRF2 inhibitors for future use.

Author's contributions

Conceptualization: XC, MBM, KPW, BW, Methodology: CP, ZX, DL, YL, BB, JC, CH, EWL, JEF, JL, KM, VC, YL, BB, HY, Funding acquisition: XC, MBM, KPW, HY, Writing original draft: CP, ZX, XC, Writing, review & editing: MBM, KPW, HY, BW.

Declaration of competing interest

The authors declare no potential conflicts of interest.

Data availability

Data will be made available on request.

Acknowledgment

This work was supported by NIH R01 CA244236 (to XC and MBM), R01 CA216051 (to MBM and BW), U54 CA156735 Full Project 5 (to XC, KPW, and MBM), U54 MD012392 Research Infrastructure Core (to XC and KPW), and Lineberger Cancer Center Development Award (to XC and HY). UNC BRIC Small Animal Imaging Facility performed ^{18}F-FDG PET/CT imaging, and the facility is partially supported by NIH P30 CA016086, and the PET/CT equipment was funded by NIH S10 OD023611. The authors would like to thank Ms. Ginger Smith (BRITE) for technical assistance and acknowledge additional support from the Golden LEAF Foundation and the BIOIMPACT Initiative of the State of North Carolina (KPW).

Appendix A. Supplementary data

Supplementary data to this article can be found online at https://doi.org/10.1016/j.redox.2023.102901.

References

[1] Y. Liu, Z. Xiong, A. Beasley, T. D'Amico, X.L. Chen, Personalized and targeted therapy of esophageal squamous cell carcinoma: an update, Ann. N. Y. Acad. Sci. 1381 (2016) 66–73.
[2] X. Kang, K. Chen, Y. Li, J. Li, T.A. D'Amico, X. Chen, Personalized targeted therapy for esophageal squamous cell carcinoma, World J. Gastroenterol. 21 (2015) 7648–7658.
[3] N. Cancer Genome Atlas Research, Analysis Working Group: asan U, Agency BCC, Brigham, Women's H, Broad I, et al. Integrated genomic characterization of oesophageal carcinoma, Nature 541 (2017) 169–175.
[4] W. Hirose, H. Oshikiri, K. Taguchi, M. Yamamoto, The KEAP1-NRF2 system and esophageal cancer, Cancers 14 (2022).
[5] E.W. Cloer, D. Goldfarb, T.P. Schrank, B.E. Weissman, M.B. Major, NRF2 activation in cancer: from DNA to protein, Cancer Res. 79 (2019) 889–898.

[6] J.D. Hayes, M. McMahon, The double-edged sword of Nrf2: subversion of redox homeostasis during the evolution of cancer, Mol. Cell 21 (2006) 732–734.
[7] B. Padmanabhan, K.I. Tong, T. Ohta, Y. Nakamura, M. Scharlock, M. Ohtsuji, et al., Structural basis for defects of Keap1 activity provoked by its point mutations in lung cancer, Mol. Cell 21 (2006) 689–700.
[8] T.W. Kensler, P.A. Egner, A.S. Agyeman, K. Visvanathan, J.D. Groopman, J. G. Chen, et al., Keap1-nrf2 signaling: a target for cancer prevention by sulforaphane, Top. Curr. Chem. 329 (2013) 163–177.
[9] A. Ohkoshi, T. Suzuki, M. Ono, T. Kobayashi, M. Yamamoto, Roles of Keap1-Nrf2 system in upper aerodigestive tract carcinogenesis, Cancer Prev. Res. 6 (2013) 149–159.
[10] M. Rojo de la Vega, E. Chapman, D.D. Zhang, NRF2 and the hallmarks of cancer, Cancer Cell 34 (2018) 21–43.
[11] M.C. Jaramillo, D.D. Zhang, The emerging role of the Nrf2-Keap1 signaling pathway in cancer, Genes Dev. 27 (2013) 2179–2191.
[12] M. Yamamoto, T.W. Kensler, H. Motohashi, The KEAP1-NRF2 system: a thiol-based sensor-effector apparatus for maintaining redox homeostasis, Physiol. Rev. 98 (2018) 1169–1203.
[13] Y. Kawasaki, H. Okumura, Y. Uchikado, Y. Kita, K. Sasaki, T. Owaki, et al., Nrf2 is useful for predicting the effect of chemoradiation therapy on esophageal squamous cell carcinoma, Ann. Surg Oncol. 21 (2014) 2347–2352.
[14] T. Shibata, A. Kokubu, S. Saito, M. Narisawa-Saito, H. Sasaki, K. Aoyagi, et al., NRF2 mutation confers malignant potential and resistance to chemoradiation therapy in advanced esophageal squamous cancer, Neoplasia 13 (2011) 864–873.
[15] X. Jiang, X. Zhou, X. Yu, X. Chen, X. Hu, J. Lu, et al., High expression of nuclear NRF2 combined with NFE2L2 alterations predicts poor prognosis in esophageal squamous cell carcinoma patients, Mod. Pathol. 35 (2022) 929–937.
[16] D. Tamborero, A. Gonzalez-Perez, C. Perez-Llamas, J. Deu-Pons, C. Kandoth, J. Reimand, et al., Comprehensive identification of mutational cancer driver genes across 12 tumor types, Sci. Rep. 3 (2013) 2650.
[17] J. Zhu, H. Wang, F. Chen, J. Fu, Y. Xu, Y. Hou, et al., An overview of chemical inhibitors of the Nrf2-ARE signaling pathway and their potential applications in cancer therapy, Free Radic. Biol. Med. 99 (2016) 544–556.
[18] N. Wakabayashi, K. Itoh, J. Wakabayashi, H. Motohashi, S. Noda, S. Takahashi, et al., Keap1-null mutation leads to postnatal lethality due to constitutive Nrf2 activation, Nat. Genet. 35 (2003) 238–245.
[19] T. Suzuki, S. Seki, K. Hiramoto, E. Naganuma, E.H. Kobayashi, A. Yamaoka, et al., Hyperactivation of Nrf2 in early tubular development induces nephrogenic diabetes insipidus, Nat. Commun. 8 (2017), 14577.
[20] C. Paiboonrungruang, E. Simpson, Z. Xiong, C. Huang, J. Li, Y. Li, et al., Development of targeted therapy of NRF2(high) esophageal squamous cell carcinoma, Cell. Signal. 86 (2021), 110105.
[21] D. Zhang, Z. Hou, K.E. Aldrich, L. Lockwood, A.L. Odom, K.T. Liby, A novel Nrf2 pathway inhibitor sensitizes keap1-mutant lung cancer cells to chemotherapy, Mol. Cancer Therapeut. 20 (2021) 1692–1701.
[22] N.D. Camp, R.G. James, D.W. Dawson, F. Yan, J.M. Davison, S.A. Houck, et al., Wilms tumor gene on X chromosome (WTX) inhibits degradation of NRF2 protein through competitive binding to KEAP1 protein, J. Biol. Chem. 287 (2012) 6539–6550.
[23] F.W. Kuhlmann, J.M. Fleckenstein, in: J. Cohen, W.G. Powderly, S.M. Opal (Eds.), Antiparasitic Agents. Infectious Diseases., Elsevier, 2017, p. 1345, 72e2.
[24] B.J. Evison, B.E. Sleebs, K.G. Watson, D.R. Phillips, S.M. Cutts, Mitoxantrone, more than just another topoisomerase II poison, Med. Res. Rev. 36 (2016) 248–299.
[25] B.M. Bowman, S.A. Montgomery, T.P. Schrank, J.M. Simon, T.S. Ptacek, T. Y. Tamir, et al., A conditional mouse expressing an activating mutation in NRF2 displays hyperplasia of the upper gastrointestinal tract and decreased white adipose tissue, J. Pathol. 252 (2020) 125–137.
[26] C.T. McHugh, J. Garside, J. Barkes, J. Frank, C. Dragicevich, H. Yuan, et al., Differences in [(18)F]FDG uptake in BAT of UCP1 -/- and UCP1 +/+ during adrenergic stimulation of non-shivering thermogenesis, EJNMMI Res. 10 (2020) 136.
[27] R.R. Ben-Harari, E. Goodwin, J. Casoy, Adverse event profile of pyrimethamine-based therapy in toxoplasmosis: a systematic review, Drugs R 17 (2017) 523–544.
[28] J.H. Zhang, T.D. Chung, K.R. Oldenburg, A simple statistical parameter for use in evaluation and validation of high throughput screening assays, J. Biomol. Screen 4 (1999) 67–73.
[29] L.N. Heppler, S. Attarha, R. Persaud, J.I. Brown, P. Wang, B. Petrova, et al., The antimicrobial drug pyrimethamine inhibits STAT3 transcriptional activity by targeting the enzyme dihydrofolate reductase, J. Biol. Chem. 298 (2022), 101531.
[30] H. Liu, Y. Qin, D. Zhai, Q. Zhang, J. Gu, Y. Tang, et al., Antimalarial drug pyrimethamine plays a dual role in antitumor proliferation and metastasis through targeting DHFR and TP, Mol. Cancer Therapeut. 18 (2019) 541–555.
[31] A. Singh, H. Wu, P. Zhang, C. Happel, J. Ma, S. Biswal, Expression of ABCG2 (BCRP) is regulated by Nrf2 in cancer cells that confers side population and chemoresistance phenotype, Mol. Cancer Therapeut. 9 (2010) 2365–2376.
[32] K. Tsuchida, T. Tsujita, M. Hayashi, A. Ojima, N. Keleku-Lukwete, F. Katsuoka, et al., Halofuginone enhances the chemo-sensitivity of cancer cells by suppressing NRF2 accumulation, Free Radic. Biol. Med. 103 (2017) 236–247.
[33] B. Harder, W. Tian, J.J. La Clair, A.C. Tan, A. Ooi, E. Chapman, et al., Brusatol overcomes chemoresistance through inhibition of protein translation, Mol. Carcinog. 56 (2017) 1493–1500.
[34] M.J. Kerins, A. Ooi, A catalogue of somatic NRF2 gain-of-function mutations in cancer, Sci. Rep. 8 (2018), 12846.
[35] D.J. Lange, M. Shahbazi, V. Silani, A.C. Ludolph, J.H. Weishaupt, S. Ajroud-Driss, et al., Pyrimethamine significantly lowers cerebrospinal fluid Cu/Zn superoxide dismutase in amyotrophic lateral sclerosis patients with SOD1 mutations, Ann. Neurol. 81 (2017) 837–848.
[36] C. Dai, B. Zhang, X. Liu, K. Guo, S. Ma, F. Cai, et al., Pyrimethamine sensitizes pituitary adenomas cells to temozolomide through cathepsin B-dependent and caspase-dependent apoptotic pathways, Int. J. Cancer 133 (2013) 1982–1993.
[37] A.M. Giammarioli, A. Maselli, A. Casagrande, L. Gambardella, A. Gallina, M. Spada, et al., Pyrimethamine induces apoptosis of melanoma cells via a caspase and cathepsin double-edged mechanism, Cancer Res. 68 (2008) 5291–5300.
[38] R. Hooft van Huijsduijnen, R.K. Guy, K. Chibale, R.K. Haynes, I. Peitz, G. Kelter, et al., Anticancer properties of distinct antimalarial drug classes, PLoS One 8 (2013), e82962.
[39] J.W. Jang, Y. Song, K.M. Kim, J.S. Kim, E.K. Choi, J. Kim, et al., Hepatocellular carcinoma-targeted drug discovery through image-based phenotypic screening in co-cultures of HCC cells with hepatocytes, BMC Cancer 16 (2016) 810.
[40] C. Tommasino, L. Gambardella, M. Buoncervello, R.J. Griffin, B.T. Golding, M. Alberton, et al., New derivatives of the antimalarial drug Pyrimethamine in the control of melanoma tumor growth: an in vitro and in vivo study, J. Exp. Clin. Cancer Res. : CR 35 (2016) 137.
[41] J.H. Matthews, X. Liang, V.J. Paul, H. Luesch, A complementary chemical and genomic screening approach for druggable targets in the Nrf2 pathway and small molecule inhibitors to overcome cancer cell drug resistance, ACS Chem. Biol. 13 (2018) 1189–1199.
[42] H.W. Hoffmanns, G. Altmeier, [Local application of mitoxantrone in inoperable, stenosing esophageal carcinoma. Preliminary report], Onkologie 9 (1986) 27–29.
[43] Y. Liu, E. Peacey, J. Dickson, C.P. Donahue, S. Zheng, G. Varani, et al., Mitoxantrone analogues as ligands for a stem-loop structure of tau pre-mRNA, J. Med. Chem. 52 (2009) 6523–6526.
[44] Y.M. Toh, T.K. Li, Mitoxantrone inhibits HIF-1alpha expression in a topoisomerase II-independent pathway, Clin. Cancer Res. 17 (2011) 5026–5037.
[45] K. Chan, R. Lu, J.C. Chang, Y.W. Kan, NRF2, a member of the NFE2 family of transcription factors, is not essential for murine erythropoiesis, growth, and development, Proc. Natl. Acad. Sci. U. S. A. 93 (1996) 13943–13948.
[46] P. Canal, M. Attal, E. Chatelut, S. Guichard, F. Huguet, C. Muller, et al., Plasma and cellular pharmacokinetics of mitoxantrone in high-dose chemotherapeutic regimen for refractory lymphomas, Cancer Res. 53 (1993) 4850–4854.
[47] M.R. de la Vega, M. Dodson, E. Chapman, D.D. Zhang, NRF2-targeted therapeutics: new targets and modes of NRF2 regulation, Curr.Opin. Toxicol. 1 (2016) 62–70.
[48] D.G. Kim, C.M. Park, S. Huddar, S. Lim, S. Kim, S. Lee, Anticancer activity of pyrimethamine via ubiquitin mediated degradation of AIMP2-DX2, Molecules 25 (2020) 2763.
[49] E.J. Choi, B.J. Jung, S.H. Lee, H.S. Yoo, E.A. Shin, H.J. Ko, et al., A clinical drug library screen identifies clobetasol propionate as an NRF2 inhibitor with potential therapeutic efficacy in KEAP1 mutant lung cancer, Oncogene 36 (2017) 5285–5295.
[50] J. Fu, Z. Xiong, C. Huang, L. Li, W. Yang, Y. Han, et al., Hyperactivity of the transcription factor NRF2 causes metabolic reprogramming in mouse esophagus, J. Biol. Chem. 294 (2019) 327–340.
[51] M.D. Coleman, G.W. Mihaly, G. Edwards, S.A. Ward, R.E. Howells, A. M. Breckenridge, Pyrimethamine pharmacokinetics and its tissue localization in mice: effect of dose size, J. Pharm. Pharmacol. 37 (1985) 170–174.